ORNL/TM-2022/2529

Printed Strain Gauges for Anthropomorphic Test Dummies for Vehicle Crash Testing
Final CRADA Report: NFE-19-07943

Peter Wang
Amiee Jackson
Tyler Smith
Vipin Kumar
Don Erdman
Rick Lowden
Kris Villez
Brenin Bales
Roo Walker

June 2022

OAK RIDGE National Laboratory

ORNL IS MANAGED BY UT-BATTELLE LLC FOR THE US DEPARTMENT OF ENERGY

ORNL/TM-2022/2529

Manufacturing Sciences Division
Advanced Manufacturing Office

PRINTED STRAIN GAUGES FOR ANTHROPOMORPHIC TEST DUMMIES FOR VEHICLE CRASH TESTING

FINAL CRADA REPORT: NFE-19-07943

Authors

Peter Wang, Amiee Jackson, Tyler Smith, Vipin Kumar, Don Erdman, Rick Lowden, Kris Villez, Brenin Bales, Roo Walker

June 2022

Prepared by
OAK RIDGE NATIONAL LABORATORY
Oak Ridge, TN 37831-6283
managed by
UT-BATTELLE LLC
for the
US DEPARTMENT OF ENERGY
under contract DE-AC05-00OR22725

CONTENTS

ABSTRACT

In Phase 1 of the technical collaboration between Oak Ridge National Laboratory (ORNL) and Humanetics, additive manufacturing was studied as a method to produce high strain – strain gauges that are embedded in an additively manufactured (AM) anthropomorphic crash test dummy (ATD) to provide high fidelity data to significantly improve vehicle safety. In this study commercially available conductive filament was acquired and the mechanical properties were tested for use in this application. The design space of embedded printed strain gauges was explored with multiple configurations printed and tested for performance. The testing resulted in finding that commercially available filament materials were unable to meet the performance requirements. Finally, an extensive literature survey was performed on advanced manufacturing techniques and novel high strain conductive materials to manufacture strain gauges that can be embedded in to the AM ATD. Humanetics have taken the literature survey and have reached out to material suppliers such as Techmer to provide custom blends of materials for testing. Humanetics will continue to build off of the research that was performed and test custom materials for use in AM ATDs.

1. BACKGROUND

This CRADA is an Oak Ridge National Laboratory Manufacturing Demonstration Facility (MDF) Technical Collaboration project with Humanetics Innovative Solutions, Inc. ORNL is a leader in manufacturing research with expertise in advanced materials, controls and analysis, modeling and advanced characterization, and systems development. Humanetics is the largest manufacturer and developer of anthropomorphic crash test dummies (ATD) in the world. Humanetics supplies ATDs in a range of sizes from new-born infants to large adults as well as assorted instrumentation, finite element models, and consultancy services.

This collaboration explores the application of additive manufacturing (AM) to integrate sensors in anthropomorphic crash test dummies (ATDs). It investigates printable material that can produce strain measurements. This material will be printed into the ATD's structure increasing the density and improving the positioning of the sensors from today's ATDs. This material must be able to withstand multiple impacts and high strain levels without degradation of sensor performance or effecting the overall stiffness of the ATD structure. The utilization of AM to produce both the structure of the ATD and the sensors will enable much greater ATD body shape and variability. This could result in a significant improvement to both crash test dummies' biofidelity and sensing fidelity, which will support the development of safer vehicles.

Recently there has been growing demand for ATDs that simulate humans of nonstandard shapes to better understand and prevent injury across a wider demographic that covers human shapes from the 5th to 95th percentile (i.e. varying weight, age, etc.). Additionally, there is a significant opportunity in embedded sensor technologies. The current state of the art dummy has 57 sensors and can measure 140 injury factors. Embedded sensors will increase the sensing capabilities by an order of magnitude allowing for detailed understanding of the loads seen on specific body parts such as specific ribs or bones due to seat belts or loads on the brain as it moves around in the skull.

Current ATDs use discrete sensors that are mounted on or into the skeleton of the dummy to measure the forces, accelerations, and deflections of different segments of the body. Currently, the dummy has available over 200 individual channels of data. Humanetics has taken the technology of constructing a dummy and adapted 3D printing technology to print skeletal components for the dummy in place of the steel structures. The 3D printed structures have been tested at different vehicle manufactures to help prove the viability of using 3D printed components in a dummy. The proposed project would enhance this technology, if it is found possible, to 3D print the strain sensors directly into the skeletal structure of the dummy. This would permit the measurement of strains directly over the skeleton to provide better mapping and capture more of the strain from the component itself and not just at the ends. If proven viable this also could be used to print sensors on substrates that could be sutured into skeletal structures of Post Mortem Human Subjects (PMHS) to achieve direct measurement of actual bone strains during testing. It would permit a better method to correlate directly with the PMHS to determine if the dummy has better human biofidelity. A successful result of this project would provide all vehicle restraint engineers with better insight to the loads on a human in an impact event and be able to develop improved countermeasures to prevent injuries. Ultimately, this would fundamentally change how dummies with sensors are manufactured. It could improve performance, reduce costs, and improve productivity by combining the 3D printed component technology with 3D printed sensors.

Beyond improving the safety of vehicles and therefore the billions of people who use them, this technology will enable the simultaneous printing of electrical and structural components of parts. This technology will enable the thousands of small machine and fabrication shops to be able to easily integrate electrical wiring and sensors into their builds without the need for specialized personnel or outsourcing

that is currently used, which will significantly expand their customer bases without significant impact to operating costs. This technology also has the potential to reduce foreign outsourcing as electronic integration is extremely labor intensive and thus often outsourced to foreign countries where labor costs are lower. The ability to produce goods under a single roof will generate significant energy savings in transportation alone by reducing the need to transport goods during manufacturing.

2. STATEMENT OF OBJECTIVES

The goal is to develop material to use as a printable strain gauge. The material must meet electrical conductivity, strength, durability, and stiffness requirements, be printable through an additive manufacturing process, and be compatible with the main structural material. ORNL will determine the minimum material requirements, identify the manufacturing method, and identify the materials to use to print the strain gauge.

3. TECHNICAL DISCUSSION

Initial Material Selection:

A survey of commercially available conductive printable filaments for additive manufacturing processes was generated. CuPLA and NinjaTek EEL were chosen. The Onyx material was originally chosen as the substrate since its mechanical properties are suitable for the application specified by Humanetics. The conductive materials were printed on to the Onyx material and found to have extremely poor bonding and a good mechanical bond could only be achieved with epoxy. Then a list of compatible substrate materials were then chosen for each conductive filament. The mechanical properties of the substrate materials were compared to the properties of Onyx. Two pairs of materials were chosen - CuPLA/PLA substrate and the NinjaTek EEL/PETG substrate. The PLA and PETG were tested with CuPLA and the EEL, respectively. These samples exhibited a stronger bond and were chosen for further testing.

***Conductive Epoxy Selection*:**

To connect flexible conductive leads to the printed samples, we used an electrically conductive epoxy. Initially, we chose Dotite D-550. However, this epoxy was difficult to apply, had a short shelf-life, was quite expensive with a long lead time, and had low mechanical strength once cured. Because of this, we evaluated using other conductive epoxies: CW2400 and Loctite Ablestik 2902. According to manufacturer's specifications, the D-550 cures to a resistivity of 0.0001 Ω-cm, while Loctite Ablestik 2902 and CW2400 both cure to 0.001 Ω-cm. After trying out all three to compare the ease of application and curing, their mechanical strength, and their cured resistivity, we decided that CW2400 would best suit our purposes. To test the curing rate of the epoxy, we created a trace of only epoxy and monitored its resistance over time after curing at 65°C for 1 hr (see Figure 1). Qualitatively, the resistance seemed to fluctuate with ambient humidity/temperature fluctuations.

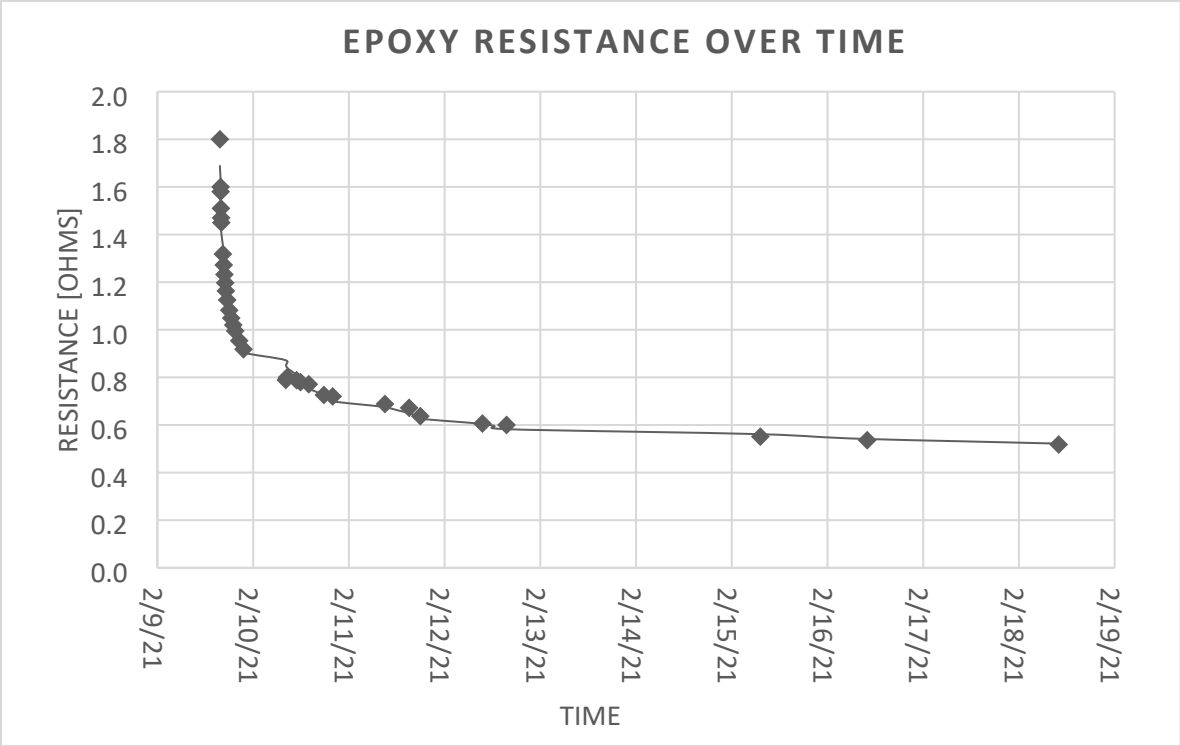

Figure 1: Data collected on resistance of conductive epoxy CW2400 as it cured over time.

Design of experiments 1: One of the first major areas of interest was in the geometry of the gauge design. Strain gauge geometry is typically comprised of the following parts:

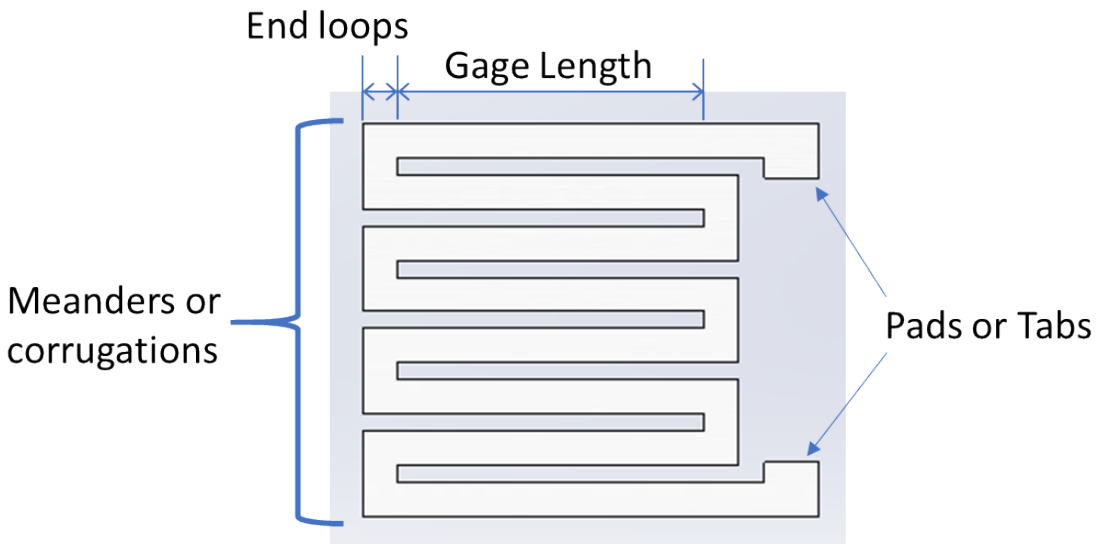

Figure 2: Major features of strain gauge geometry whose operating principle is based on change in resistance.

Design of Experiment: In this round of testing, 16 unique sample variations were generated by varying four parameters between two possible values. The parameters varied were materials, number of corrugations, gauge length, and print orientation/strategy. The materials were either the PLA with CuPLA combination or the ESD PETG with NinjaTek EEL combination. There were either 2 or 4 meanders, with one additional successfully printed instance of a 6 meander geometry printed from PETG with EEL. The gauge lengths were either 20 or 30mm. Samples had either surface or embedded gauges. For surface gauges, the entire base was printed first and then the gauge was printed on top. In this way, the orientation while printing was such that the face with the largest surface area contacted the print bed. For the embedded gauges, both substrate and conductive materials were deposited in each layer, and the part orientation while printing was such that the face with the second greatest surface area contacted the print bed. The overall dimensions of the base for these gauges was informed by the thickness and width of the rib geometry provided by Humanetics. The gauge length values were selected to fit eight gauges along the rib geometry with more or less gap in between each gauge.

Sample Preparation: The exact dimensions of meander width and height, end loop width, and pad length and width were constrained to be integer multiples of the bead width or layer height on the printer used. The printer used for all samples was a MakerGear m3-id. After printing and verifying a continuous conductive path in the printed sample, conductive leads made from folded copper tape were attached to the samples with the CW2400 conductive epoxy. The epoxy was cured at 65°C for about 1hr on the print bed. In the printing process, about a dozen iterations of printing was required to tune the printing parameters for each material combination, with further tweaks required between the surface and embedded iterations. Some of the main issues observed during printing were: lack of adhesion between the substrate and conductive materials, lack of self-adhesion for conductive materials, stringing between stops and starts of beads, and filament feedstock embrittlement as correlated with humidity absorption over time. When not actively printing with a material for more than a day, the material was dried in a

furnace well below 100°C for at least 8 hours. Once dialed in, the same printing parameters were used for all gauges of the same material and orientation.

Testing and Data Collection: Sample testing took place in the Experimental Mechanics Lab on a tensile testing machine built and developed by the lab, shown in Figure 2.

Figure 3: Tensile testing machine at Experimental Mechanics Lab, with a sample loaded and extensometer affixed.

The extensometer used was the MTS 634.11E-25, which was attached to the sample with rubber bands (see Figure 4). The extension, machine displacement, and force data were logged using a custom LabView project for the tensile testing machine. The multimeter used was a Keithley 2110, and the data was collected with the Keithley logging software (see Figure 5). Because two different logging systems were used, we attempted to synchronize the start time with a verbal countdown till start.

To resolve asynchronous data sampling from the two data logging systems, we leveraged the Nadaraya-Watson kernel-weighted average, with a triweight kernel strategy to smooth and interpolate a synchronous dataset. With this dataset, we plotted strain against the normalized change in resistance. For some datasets, the resistance in a no-stress state between cycles decreased from cycle to cycle (termed zero drift), while in others it remained relatively constant. For those where it remained relatively constant, the normalized change in resistance was calculated as $(R_{measured} - R_{static})/R_{static}$. For those where zero drift was observed, the normalized change in resistance was calculated as $(R_{measured} - R_{cycleLocalMin})/R_{cycleLocalMin}$.

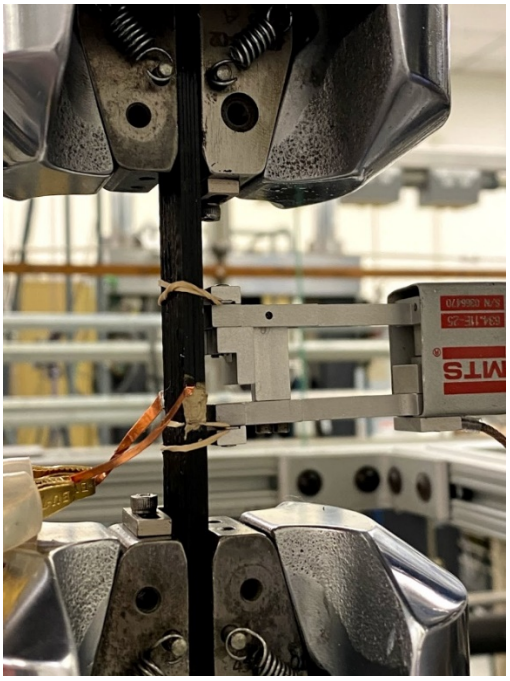

Figure 4: Detail view of sample loaded in grips (center), multimeter leads attached (left) and extensometer affixed (right), ready for testing.

Figure 5: Multimeter (right) and resistance data logging software (left) used, as set up in the Experimental Mechanics Lab.

Each CuPLA with PLA sample was cycled from its initial resting state to a 0.5mm displacement and back five times. Each EEL with PETG sample was cycled from its initial resting state to a 0.5mm displacement and back five times, followed by another set of displacement cycles to 1mm and back. The rate of displacement for all samples was 0.001in/sec. For all samples, in between each cycle the bottom clamp on

the machine was opened for approximately 3 seconds to allow the sample to relax. We observed that just having both clamps closed caused 12-13 lbs of compression on any given sample. During testing, we also observed delamination on the surface printed gauges between the base material and the gauge material. Some samples we noticed had an initial bow and weren't exactly flat prior to testing. Some samples bowed in testing as the grips returned to their initial position. Some samples broke during testing as well.

Results and Trends: Two parameters qualitatively had the greatest impact on gauge performance: material and orientation. Observations on gauge performance can cluster the samples into four groups with commonalities based on these parameters: 1) surface CuPLA with PLA; 2) embedded CuPLA with PLA; 3) surface EEL with PETG; and 4) embedded EEL with PETG.

Common characteristics in performance from group 1 included:

- There was significant zero-shift downward from cycle to cycle.
- First peak amplitude in resistance was much greater than other peak amplitudes.
- Variance in resistance amplitude was correlated to the variance in extensometer strain amplitude.
- Between cycles, the measured resistance didn't return to a stable value—it decreased with time each time.

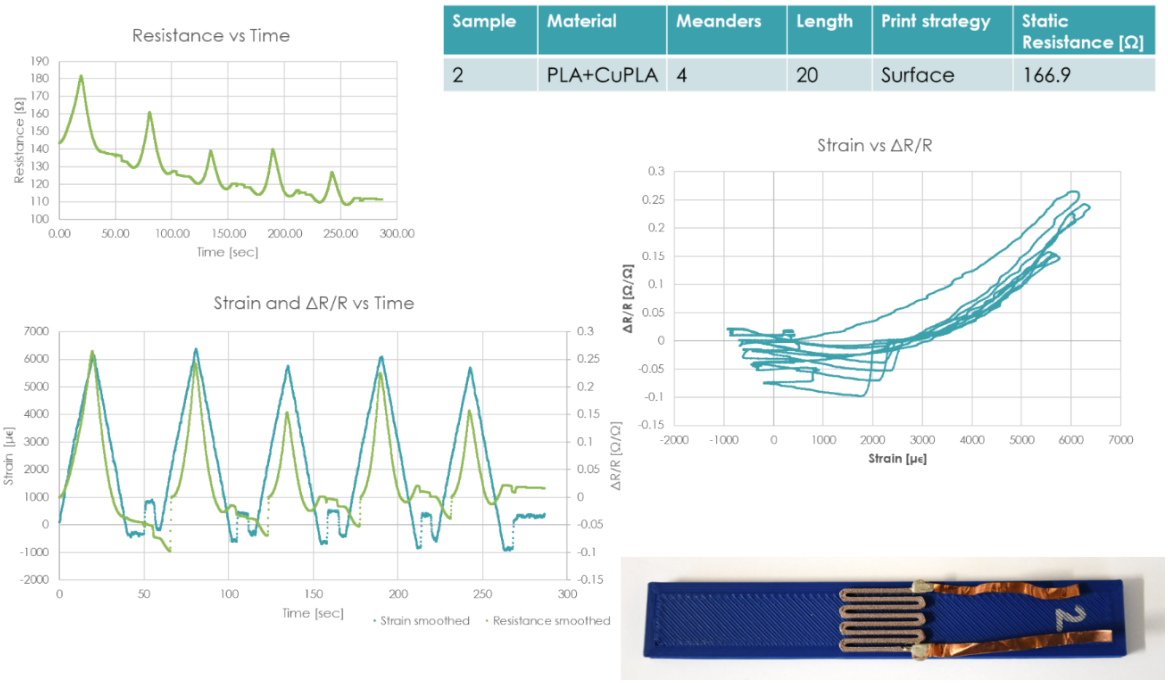

Sample	Material	Meanders	Length	Print strategy	Static Resistance [Ω]
2	PLA+CuPLA	4	20	Surface	166.9

Figure 6: Representative example of one sample from group 1.

Common characteristics in performance from group 2 included:

- There was very little zero-shift downward from cycle to cycle.
- First peak amplitude in resistance was much greater than other peak amplitudes.
- Between cycles, the measured resistance returned to a more stable value than in group 1.
- As the number of cycles increased, the variance in amplitude decreased.

Sample	Material	Meanders	Length	Print strategy	Static Resistance [Ω]
18A	PLA+CuPLA	4	30	Embedded	666

Original sample is pretty bowed

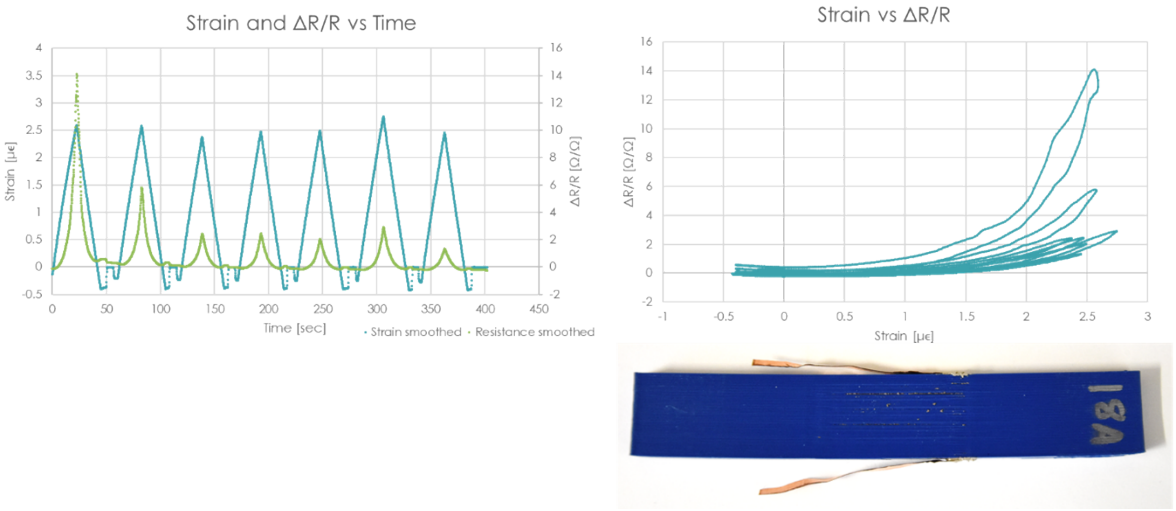

Figure 7: Representative example of one sample from group 2.

Common characteristics in performance from group 3 included:

- The resistance response of both samples with 2 meanders seemed to be inverted.
- Very strange behavior in resistance between cycles, where the resistance increased significantly when it was expected to decrease.

Was very easy to delaminate gauge from base after test

Sample	Material	Meanders	Length	Print strategy	Static Resistance [Ω]
7	PETG+EEL	2	20	Surface	1211.2

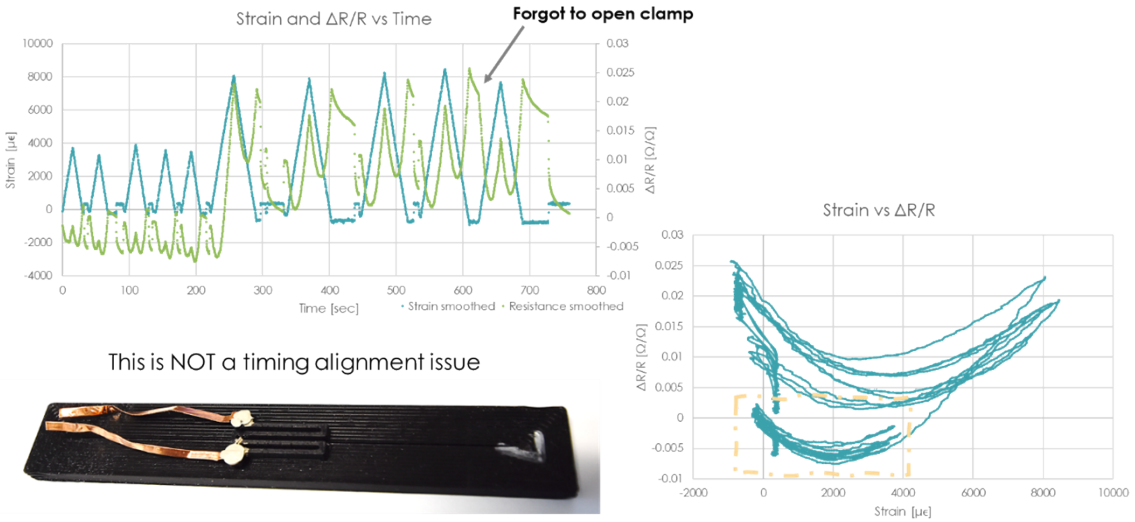

Figure 8: Representative example of one sample from group 3.

Common characteristics in performance from group 4 included:

- Three samples of the five tested broke during the 1mm displacement cycles.
- Three samples of the five tested showed promising data during the 0.5mm cycles.
- Failure occurred where there were visible printing defects at the interfaces between conductive and dielectric materials in this sample set.

Sample	Material	Meanders	Length	Print strategy	Static Resistance [Ω]
P38	PETG+EEL	4	30	Embedded	50217

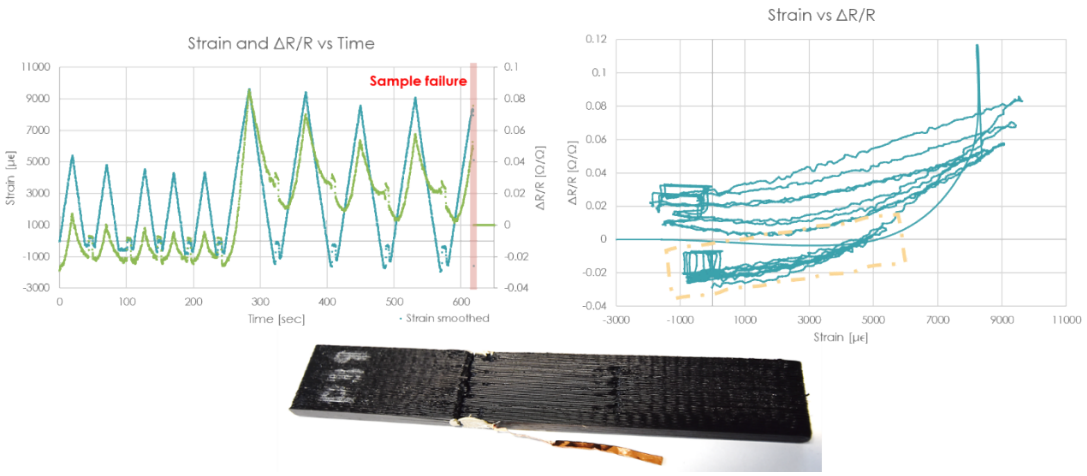

Figure 9: Representative example of one sample from group 4.

In summary, the trends in observations that were identified across our sample set were that the surface gauges exhibited significantly more zero drift than the embedded gauges. We hypothesize this was due to delamination between the conductive and dielectric materials. The PETG with EEL surface samples exhibited the strangest response in resistance to strain, with some instances of negative slope on the strain vs resistance graph. This can be seen graphically where the trends on the other three groups of samples are all either zero or positive slope, while the trend on group 3 is reminiscent of the letter "u".

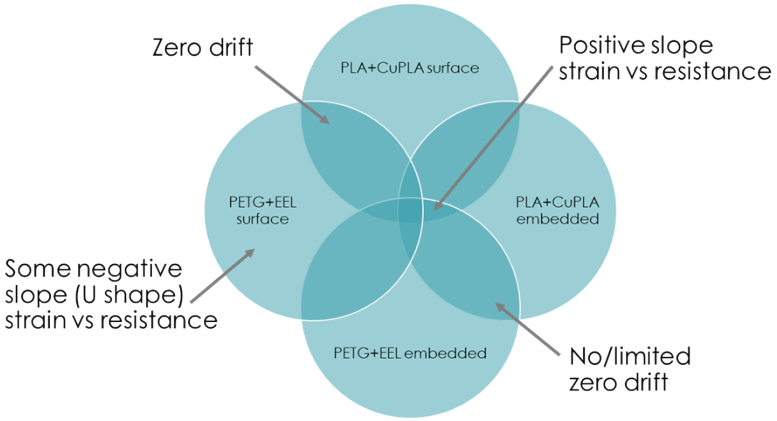

Figure 10: Venn diagram of common and unique trends from the four groups described.

Conclusions: Four parameters were varied in this experiment: number of meanders, gauge length, materials, and print orientation. The materials and print orientation had the greatest impact on sensor performance. Printing parameters also played a critical role, where some sensors failed due to poor printing quality. Sensors with more meanders had a higher static resistance than those with fewer meanders. However, those with greater gauge length did not necessarily have higher static resistance than those with shorter gauge length. Because of this, we hypothesize that the number of end loops adds more resistance than the length of gauge. This may be due to inconsistent cross-sectional areas at or near the end loops due to printing parameters.

Moving forward, we decided to iterate further on printing parameter development, design for embedded sensors only, and test for sensor repeatability.

Design of experiments 2: The main motivation in this round of testing was to learn about gauge repeatability.

Design of Experiment: In this round of testing, 15 samples were generated for testing sensor repeatability. All samples were embedded, and two different printing orientations were considered, as well as three material combinations. The printing orientations considered are shown in Figure 11:

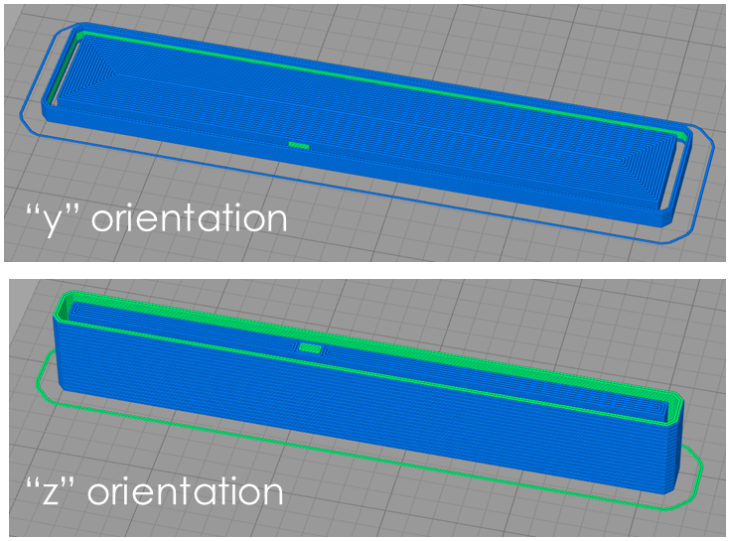

Figure 11: The two printing orientations tested. Above: y-orientation. Below: z-orientation.

The materials combinations considered are PLA with CuPLA, ESD PETG with NinjaTek EEL, and 3DXMAX PETG with NinjaTek EEL. We chose to use two different types of PETG in order to compare their printability and see if there were significant differences in their performance. The overall dimensions of the base geometry were informed by the thickness and width of the rib geometry provided by Humanetics. The gauge length chosen was 20mm, as this was deemed the most realistic fit for a total of 8 gauges in each beam on each side of the rib geometry. The same gauge geometry was used for all samples; the meander width and height selected were constrained to be the least common multiple of the printed bead width and layer height respectively. At least three samples of the same material combination were printed in the z-orientation, and at least one sample of the same material combination in the y-orientation.

Sample Preparation: The process followed for preparing the samples was largely the same as the first round of testing. For each sample orientation and material combination set, the same .gcode and printing parameters was used for the samples, in order to test for repeatability. Again, drying the materials (particularly the EEL filament) prior to printing significantly improved printability. The curing process for the conductive epoxy took place in a furnace at about 75C for about 10-15 minutes. To secure the leads while the epoxy was still in its uncured state (and during curing), a heat-resistant tape was wrapped around the sample after applying the epoxy.

Testing and Data Collection: The equipment used in this round of testing was the same as the first. The same strategy was leveraged to interpolate synchronous data from the two data streams, this time via a custom Python script. Each sample was stretched up to 0.5mm and back for at least 25 cycles at a rate of

0.001in/sec. The bottom clamp was opened between each cycle for approximately 3 seconds to allow the sample to relax unconstrained. We observed a 20-70lbs compression load accumulate when the grips were returned to their original position depending on the sample.

Results and Trends: The static resistance of each gauge was measured on the day of testing prior to testing, as well as a few days afterward. This static resistance decreased from before to after for every sample tested. The samples can be grouped into three main groups based on material combinations, with two subgroups per group based on print orientation: 1.1) CuPLA with PLA in the y-orientation; 1.2) CuPLA with PLA in the z-orientation; 2.1) ESD PETG with EEL in the y-orientation; 2.2) ESD PETG with EEL in the z-orientation; 3.1) 3DXMAX PETG with EEL in the y-orientation; and 3.2) 3DXMAX PETG with EEL in the z-orientation. We decided to include in our analysis a graph of microstrain and resistance vs time, with an overlay of red or blue where the sample was in tension or compression respectively based on the load cell measurements at that time as well. It is of note that the resistance values increased while the sample experienced a compressive load. For many samples we also selected the local maxima in resistance, load, and strain from each cycle and plotted their values against time. This second plot demonstrates visually how the resistance signal correlates to the differences in load and strain conditions experienced by the sample.

Common characteristics in performance from group 1.1 are:

- There was significant zero-shift downward from cycle to cycle; the zero-shift decreased and levelled out as the number of cycles increased.
- First peak amplitude in resistance was much greater than other peak amplitudes; the resistance peak amplitudes became more consistent as the number of cycles increased.
- Variance in resistance amplitude was correlated to the variance in extensometer strain amplitude.

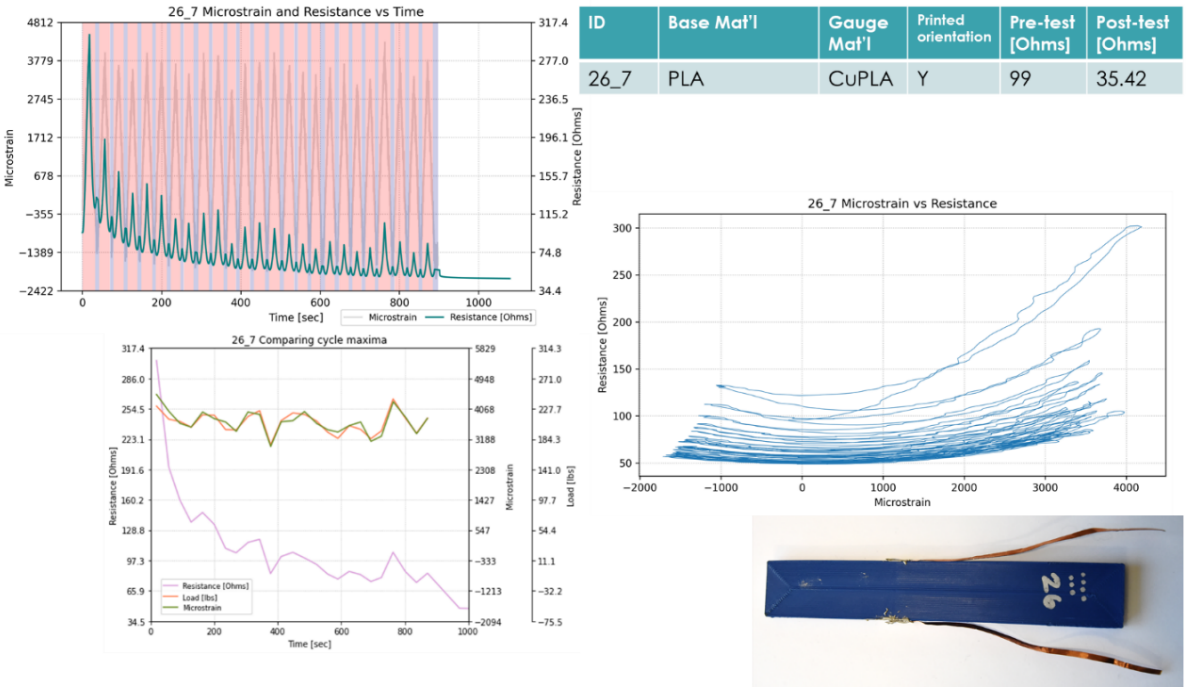

ID	Base Mat'l	Gauge Mat'l	Printed orientation	Pre-test [Ohms]	Post-test [Ohms]
26_7	PLA	CuPLA	Y	99	35.42

Figure 12: Representative example of sample from group 1.1.

Common characteristics in performance from group 1.2 are:

- First peak amplitude in resistance was much greater than other peak amplitudes; the resistance peak amplitudes became more consistent as the number of cycles increased.
- Variance in resistance amplitude was correlated to the variance in extensometer strain amplitude.
- Zero-shift is less pronounced downward for three of four samples as compared to group 1.1.

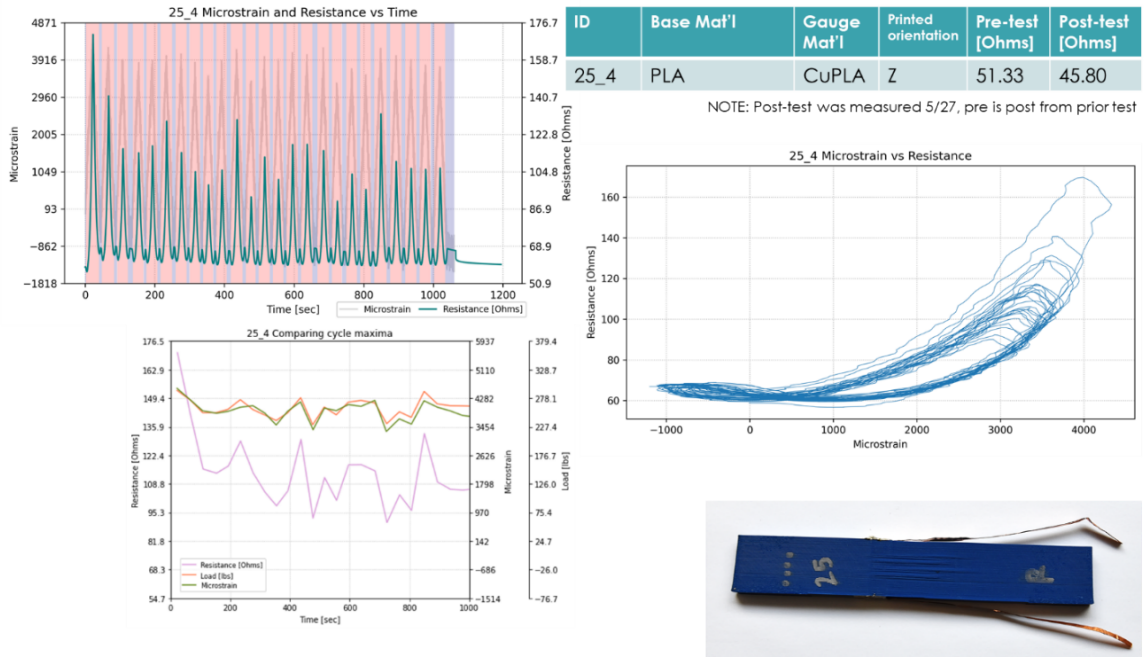

ID	Base Mat'l	Gauge Mat'l	Printed orientation	Pre-test [Ohms]	Post-test [Ohms]
25_4	PLA	CuPLA	Z	51.33	45.80

NOTE: Post-test was measured 5/27, pre is post from prior test

Figure 13: Representative example of one sample from group 1.2.

Common characteristics in performance from group 2.1 are:

- Resistance peak in tension is significantly higher than in compression.
- Variance in resistance amplitude was correlated to the variance in extensometer strain amplitude.
- Notable zero-shift from cycle to cycle; appears somewhat linear.

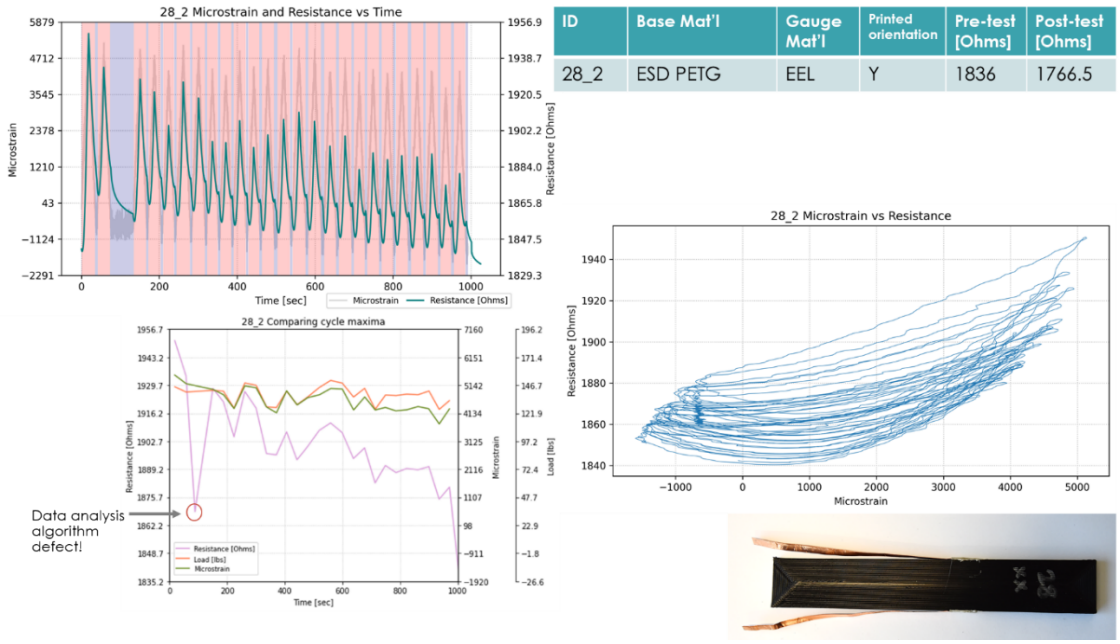

ID	Base Mat'l	Gauge Mat'l	Printed orientation	Pre-test [Ohms]	Post-test [Ohms]
28_2	ESD PETG	EEL	Y	1836	1766.5

Figure 14: Representative example of one sample from group 2.1.

Common characteristics in performance from group 2.2 are:

- Resistance peak in tension is roughly equal to or less than the peak in compression for many cycles. This effect worsens as cycles accumulate.
- Notable zero-shift from cycle to cycle; appears somewhat linear.
- Variance in resistance amplitude was correlated to the variance in extensometer strain amplitude.

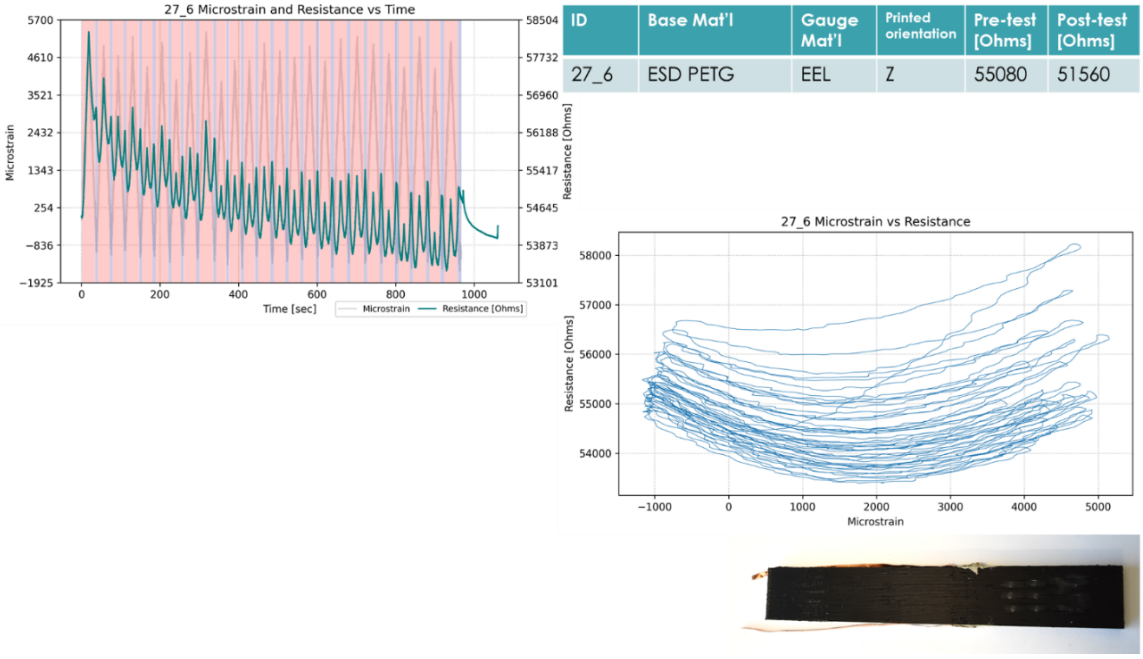

ID	Base Mat'l	Gauge Mat'l	Printed orientation	Pre-test [Ohms]	Post-test [Ohms]
27_6	ESD PETG	EEL	Z	55080	51560

Figure 15: Representative example of one sample from group 2.2.

Common characteristics in performance from group 3.1 are:

- Resistance peak in tension is significantly higher than in compression.
- Variance in resistance amplitude was correlated to the variance in extensometer strain amplitude.
- Notable zero-shift from cycle to cycle; appears somewhat linear.

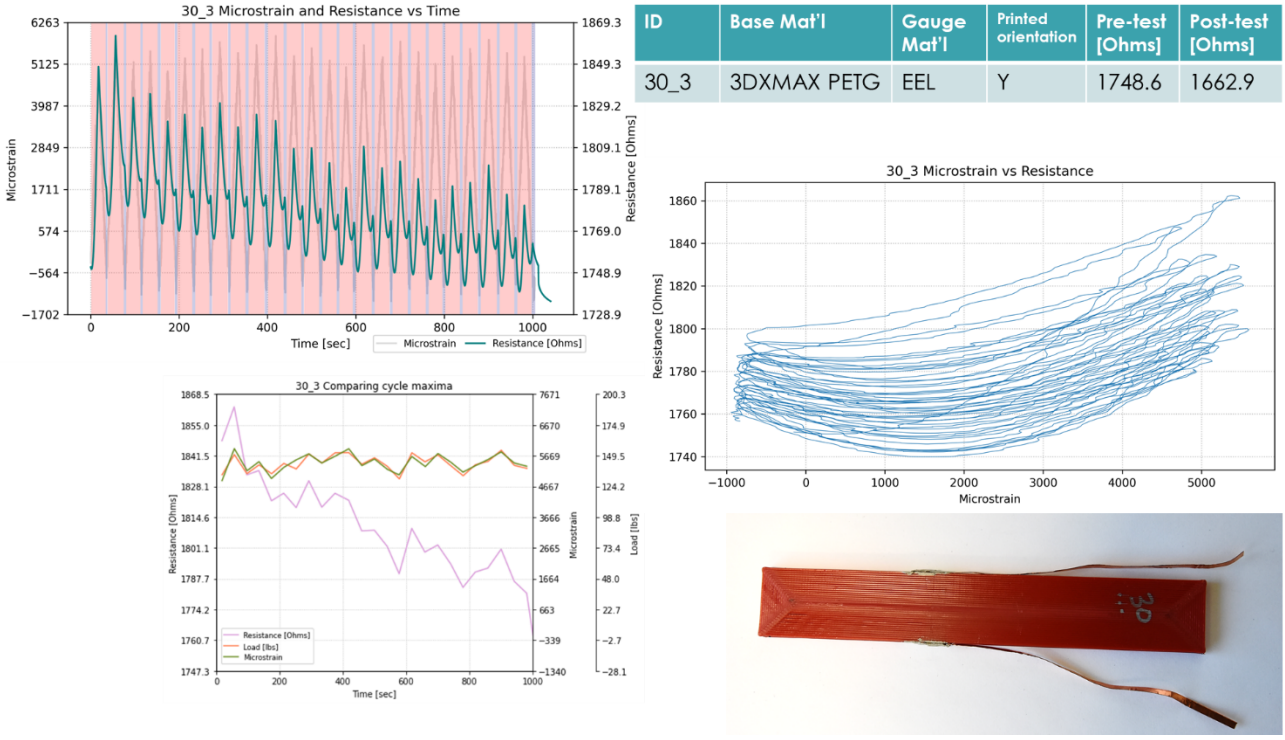

ID	Base Mat'l	Gauge Mat'l	Printed orientation	Pre-test [Ohms]	Post-test [Ohms]
30_3	3DXMAX PETG	EEL	Y	1748.6	1662.9

Figure 16: Representative example of one sample from group 3.1.

Common characteristics in performance from group 3.2 are:

- Resistance peak in tension is on the same order of magnitude or roughly equal to the peak in compression for many cycles. This effect worsens as cycles accumulate.
- Notable zero-shift from cycle to cycle; appears somewhat linear.
- Variance in resistance amplitude was correlated to the variance in extensometer strain amplitude.

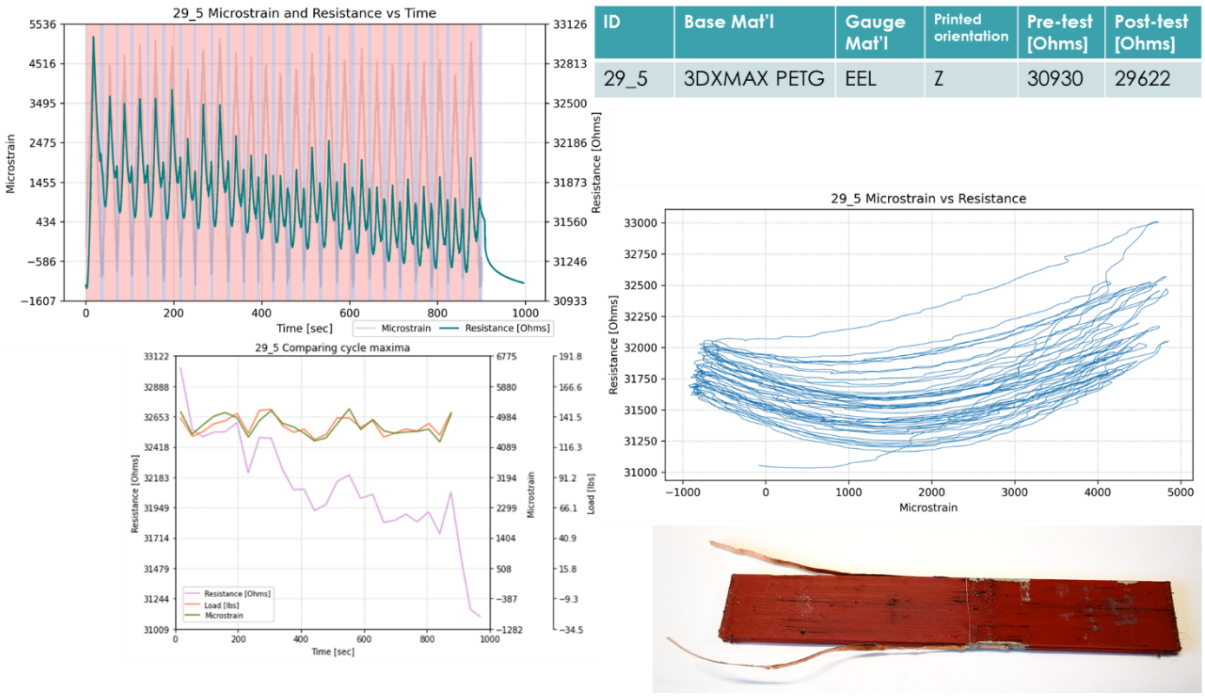

ID	Base Mat'l	Gauge Mat'l	Printed orientation	Pre-test [Ohms]	Post-test [Ohms]
29_5	3DXMAX PETG	EEL	Z	30930	29622

Figure 17: Representative example of one sample from group 3.2.

In summary, the trends in observations that were identified across our sample set were that those printed in the y-orientation exhibited a lower resistance and lower initial cycles spike in resistance than those printed in the z-orientation. The amplitude of the resistance spike when the sample was in compression was also smaller in comparison to the amplitude of the resistance spike when the sample was in tension for those printed in the y-orientation. The samples printed in the z-orientation exhibited a resistance spike when the sample was in compression that was roughly equal to or greater than the amplitude of the resistance spike when the sample was in tension.

Those samples printed in PLA with CuPLA exhibited the lowest resistance range and the highest load range. In their response, the zero shift seemed to converge more quickly and in fewer cycles than the PETG with EEL based samples. In general, those printed from PLA with CuPLA had resistance peaks in compression that were less than and much less than the peaks during tension. The samples printed in ESD PETG with Ninjatek EEL exhibited the highest resistance range. The load and strain range with ESD PETG with Ninjatek EEL was comparable to the load and strain range with 3DXMAX PETG with Ninjatek EEL. The zero shift in both PETG based combinations converged less quickly than the PLA based material combination. The resistance peaks in compression were comparable to or greater than the resistance peaks in tension for the PETG based material combinations as well. The greatest difference between the PETG combinations was the resistance range for the 3DXMAX PETG combination was slightly lower than that of the ESD PETG combination.

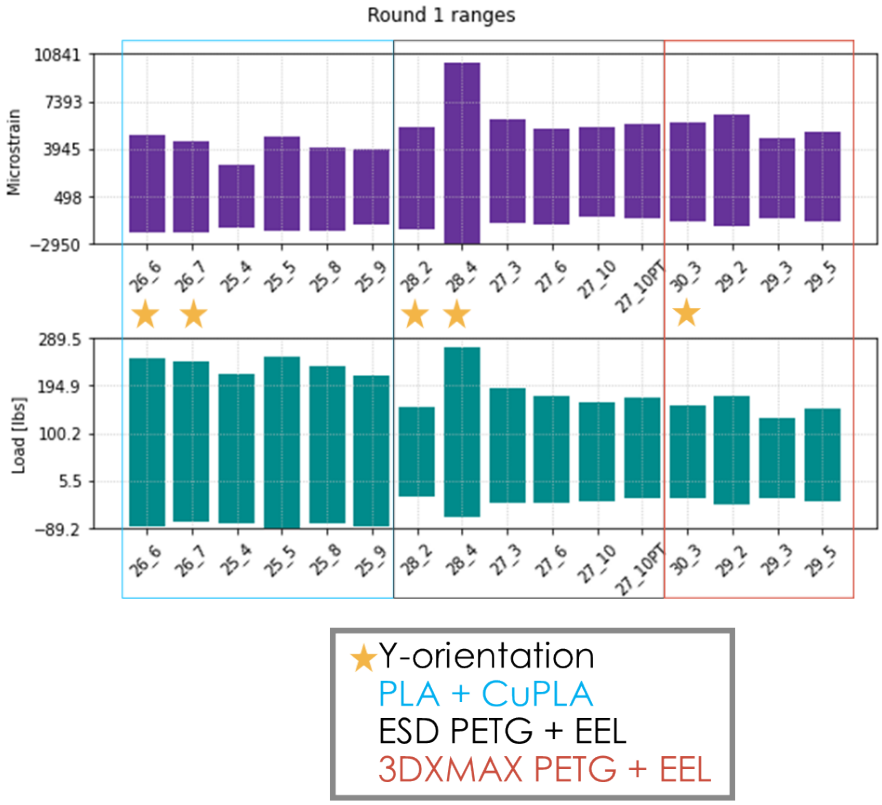

Figure 18: Microstrain and load ranges tested for each sample. Samples are grouped by material combination, with a star denoting which were printed in the y-orientation. Those not printed in the y-orientation were printed in the z-orientation.

Conclusions: This round of testing set out to investigate gauge repeatability. This was tested by creating duplicates of samples and testing them for more cycles than the prior round. We observed that for many samples the repeatability to itself improves with more cycles. We observed some variance in performance from sample to sample within those of the same material and printed orientation. However, we saw commonalities in performance that were approximately group specific.

Bonus Experiments: We observed some unexpected phenomena during testing, specifically the existence of compression during the testing cycle as well as drastic increases in resistance during compression. These observations sparked further testing to better understand these phenomena. We tested to determine the recovery or relaxation rate of the material, to see what pre-tensioning the sample would do, to try different strain rates and amplitudes, and to see how the samples responded in compression.

Sample Preparation: For these tests, some of the samples from the prior set were used after the testing from the prior set was completed. Other samples used were the best of those deemed not good enough for the prior set of testing. Eleven samples in total were tested, with four of these having been used for the prior set of testing. The preparation process for these samples was the same as those for the second round of testing.

Testing and Data Collection: The same testing equipment was used for all of these bonus experiments. The same data logging and Python script for synchronous data interpolation was used for this data. Procedures that were specific to each experiment will be elaborated on for each individually.

Recovery Rate Test:

Testing Procedures: First, the bottom clamp was opened and the sample was allowed to relax. A relaxed sample was indicated to the testers by a relatively stable resistance reading. Once relaxed, the bottom clamp was closed. Then the test was started, with the software set to trigger and then hold, rather than trigger and then return as used for the cyclic method of testing. Once the trigger condition was achieved and the grips were no longer in motion, the bottom clamp was opened. With the bottom clamp opened, the grips were returned to their initial position and the sample resistance monitored while it relaxed. This procedure was repeated 6-10 times per sample. For one sample, the trigger was programmed to be 0.5mm displacement with a ramp rate of 0.001in/sec. For the other two tests, the trigger was programmed to be 2000 microstrain with a ramp rate of 0.0005in/sec. One of the samples was ESD PETG with EEL, while the other was 3DXMAX PETG with EEL.

Results: The resistance vs time since release was plotted and curve fit for each cycle. The curve fits are shown in the diagrams to the left, with all decays shown overlaid in the plot on the right of Figure 19.

ID	Base Mat'l	Gauge Mat'l	Printed orientation	Pre-test [Ohms]	Post-test [Ohms]
29_5	3DXMAX PETG	EEL	Z	30930	29622

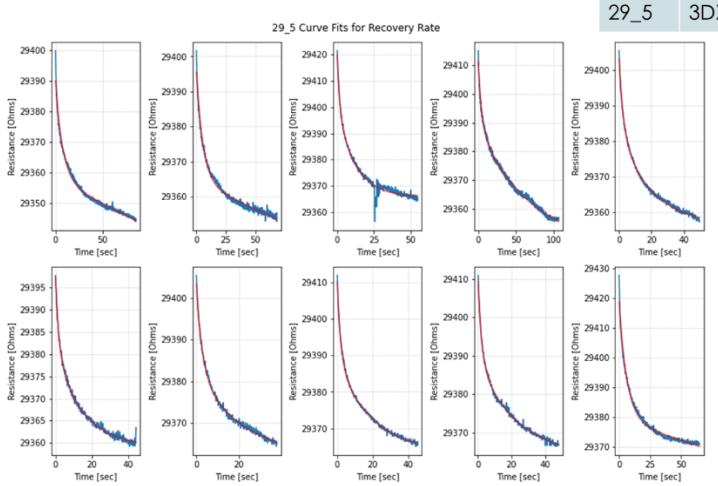

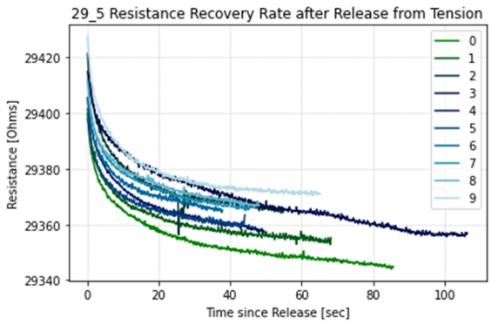

Figure 19: One set of results from one sample in the recovery rate tests.

A bi-exponential decay equation was used to curve fit: $y = a_1 e^{-b_1 x} + a_2 e^{-b_2 x} + c$. The red line in the resistance vs time graphs toward the left of figure is the curve fit line, while the blue is the data itself.

Conclusions: The resistance of the PETG with EEL-based samples does not return to its original value in an unstressed state in a linear fashion. Rather, the resistance decreases in some form of exponential decay when released approximately instantaneously from a tensile stress state.

Pre-tensioned Test:

Testing Procedures: First, the sample was positioned and the grips were closed as normal. Then, the sample was manually pre-tensioned to 35lbs. Next this pre-tensioned state was set as "zero" load in the software. Then, cycles to 0.5mm displacement at a ramp rate of 0.001in/sec were performed as normal. This test was done after all of the repeatability testing.

Results: Microstrain and resistance vs time, with tensile and compressive load ranges overlaid in red and blue, respectively, is show in the bottom plot of Figure 20. The top plot shows the resistance vs microstrain plot, which depicts significant negative slope regions below 2000 microstrain.

ID	Base Mat'l	Gauge Mat'l	Printed orientation	Pre-test [Ohms]	Post-test [Ohms]
27_10	ESD PETG	EEL	Z	64600	58280

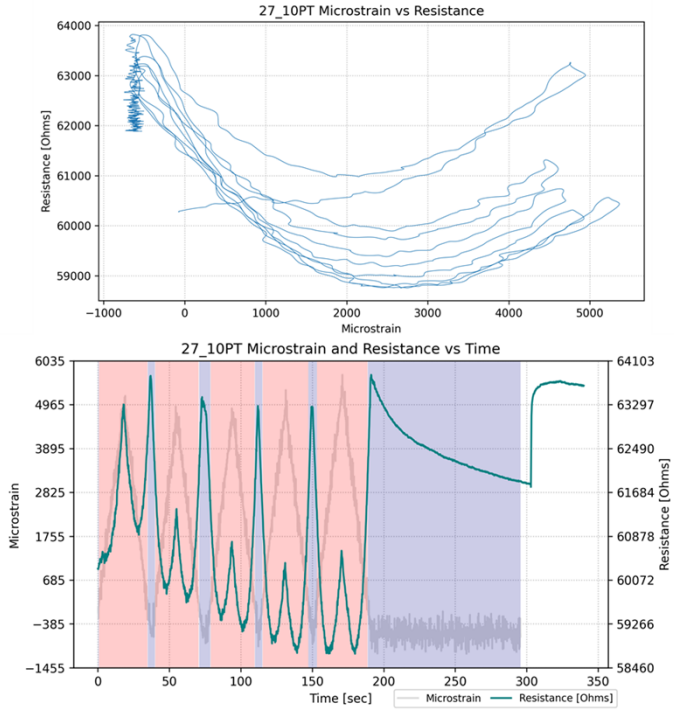

Figure 20: Pre-tensioned test results.

There is notable zero-shift in the resistance data, with the resistance peaks during compression far surpassing the resistance peaks during tension. The first resistance peak in tension has a greater amplitude than the following four.

Conclusions: Based on our observations, pre-tensioning the sample at 35lb does not effectively reduce or eliminate the compression ranges nor the large spikes in resistance during these ranges.

Varying Cycle Amplitudes Test:

Testing Procedures: All methods of cyclic testing were the same as for the repeatability tests, except the trigger value was changed. For the first seven cycles, the trigger was set to 1mm displacement. For the remaining 18 cycles, the trigger was set to 0.75mm.

Results: Plots of resistance vs microstrain (left) and microstrain and resistance with tension and compression overlay vs time (right) are shown in Figure 21.

ID	Base Mat'l	Gauge Mat'l	Printed orientation	Pre-test [Ohms]	Post-test [Ohms]
28_4	ESD PETG	EEL	Y	2009	1812.7

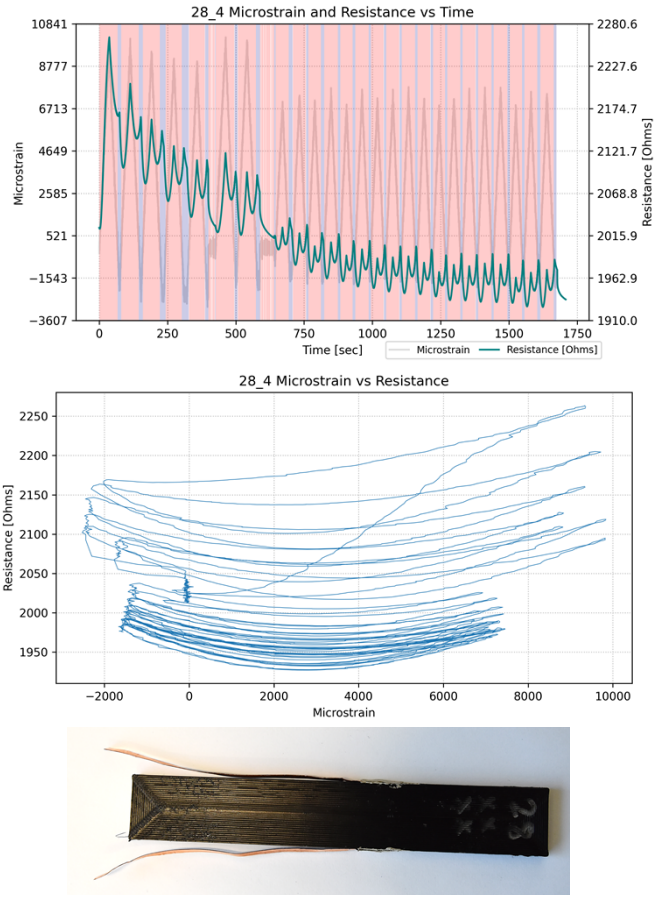

Figure 21: Varying cycle amplitudes test results.

There is notable zero shift, which appears to be more pronounced in the 1mm cycles than in the 0.75mm cycles. The severity of the compression peaks relative to the tension peaks appears to worsen as the number of cycles increases.

Conclusions: The compression zones are not mitigated or eliminated at cycle amplitudes up to double the displacement as tested in the repeatability or geometric variations trials.

Compression Test:

Testing Procedures: One sample of each material combination was tested. The same set-up was used as the repeatability testing, but the trigger was changed to a compressive load. For the PLA with CuPLA sample, the trigger load was set to 110lbs with a ramp rate of 0.001 in/sec. For the PETG with EEL based combinations, the trigger load was set to 50lbs with a ramp rate of 0.0005 in/sec. All samples tested had been printed in the z-orientation. It should be noted that the samples tested had a slenderness ratio of approximately 21:1, which is well above the recommended range of ratios of 11:1 to 16:1 [1]. Thus, what is termed "compression" here may be buckling phenomena.

Results: Plots of resistance and microstrain vs time with tension and compression overlays (left) and resistance vs microstrain (right) are shown in Figure 22.

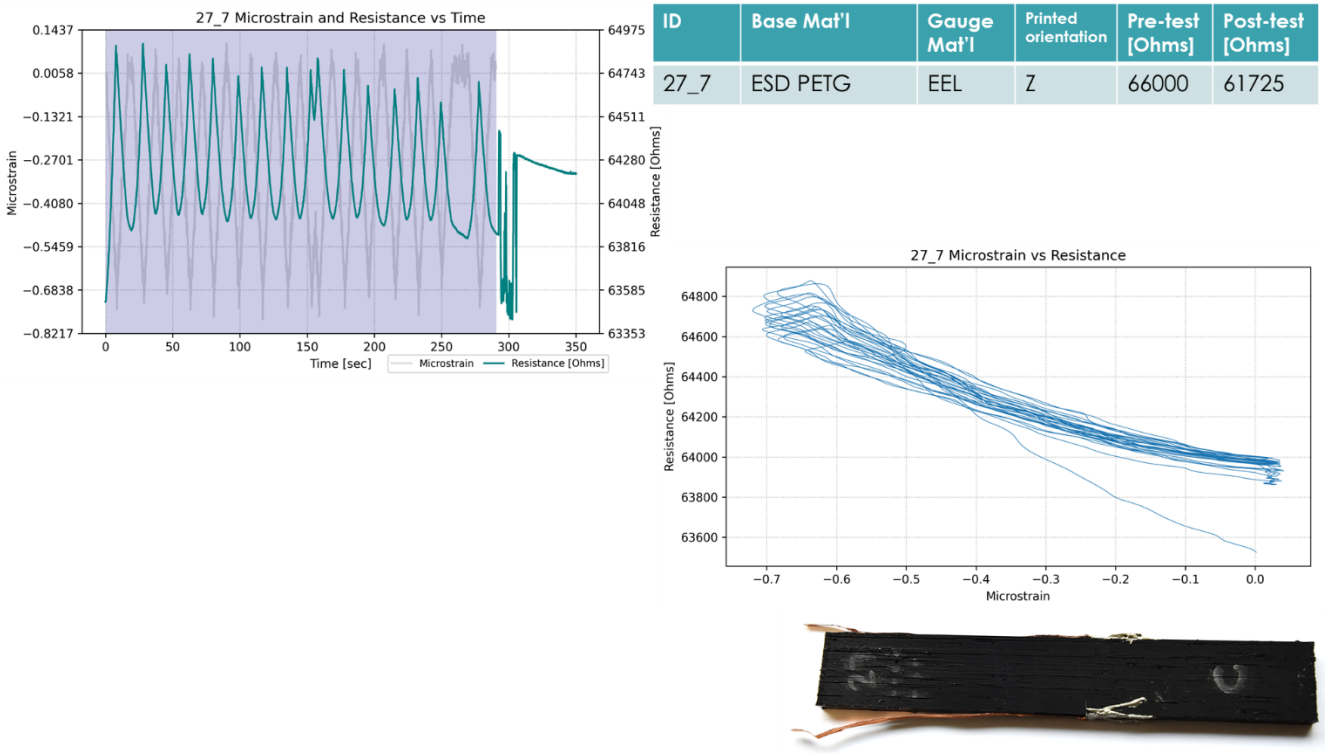

ID	Base Mat'l	Gauge Mat'l	Printed orientation	Pre-test [Ohms]	Post-test [Ohms]
27_7	ESD PETG	EEL	Z	66000	61725

Figure 22: Representative example of one sample from compression testing.

For the ESD PETG with NinjaTek EEL samples, the resistance vs microstrain graph appears to be consistently linear with a negative slope. The PLA with CuPLA sample exhibited zero shift. The 3DXMAX PETG with NinjaTek EEL sample had quite noisy data, but still showed a roughly linear resistance vs microstrain graph with consistent negative slope. Neither of the PETG with EEL based material combinations exhibited significant zero-shift in these tests.

Conclusions: A compressive load exerted on the sample geometry results in increasing resistance. Bending or buckling behavior may play an important role in this phenomenon.

Slower Rates and Lower Strain Tests:

Testing Procedures: The testing procedures were largely identical to those followed for the repeatability tests, except the trigger for these tests was set to 2000 microstrain, with a ramp rate of 0.0005in/sec for three of the four sets and a ramp rate of 0.001in/sec for the fourth. One sample of each material combination was tested, and all three selected had been printed in the y-orientation. The sample shown in figure 17 was tested first at the slower ramp rate, and then at the faster ramp rate. None of these samples had been tested prior.

Results: Plots of microstrain and resistance with compression and tension overlays vs time (left) and resistance vs microstrain (right) are shown in Figure 23.

The slow test was done just prior to the fast test

ID	Base Mat'l	Gauge Mat'l	Printed orientation	Pre-test [Ohms]	Post-test [Ohms]
28_1	ESD PETG	EEL	Y	2296	2180.7

NOTE: Post-test was measured 5/27, pre is from 5/3

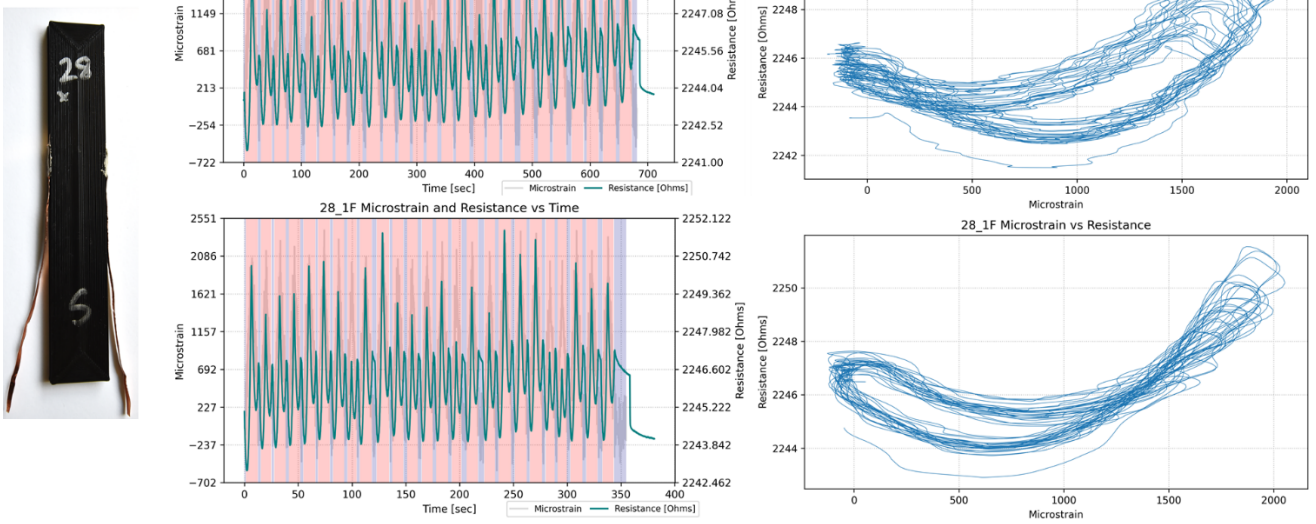

Figure 23: Representative sample from varying strain rate at lower strain amplitude. Above: slower rate; Below: faster rate.

The correlation between amplitude of microstrain cycles and amplitude of resistance cycles appears to be less consistent than seen in other tests. The PLA with CuPLA sample exhibited significant zero drift. The compression peaks were consistently differentiable from the tension peaks.

Conclusions: Cycling the samples at the slower strain rate or to lower amplitude strain does not eliminate the resistance spike in compression between strain cycles. The slow rate selected for this test was the slowest realistically possible for the tensile testing machine used. Interest remains for testing slower rates yet, but a different tensile testing machine would be required.

Mechanical Testing

Design of Experiment: The mechanical properties of PLA, PETG, CuPLA and EEL were measured via ASTM 638 tensile samples. The hypothesis was that a significant difference between the conductive polymers and the base material contributed to the anomalous behavior observed in the previous experiments. If the conductive materials were plastically deforming while the base materials were not, the sensor output would have been affected. Mechanical properties of all the printed materials were not readily available. Five samples of each material and orientation (x and z: parallel to and orthogonal to the slice plane, respectively) were prepared for testing. Ten samples of the CuPLA x-orientation were prepared. The x-orientation samples are those whose longest axis aligns with the printing direction within a layer and does not cross interlaminar boundaries. The z-orientation samples are those whose longest axis crosses interlaminar boundaries.

Sample Preparation: Samples were created by printing a triangular extrusion, cutting the faces apart at the vertices with a bandsaw, then cutting out ASTM 638 samples with a waterjet from each panel (see Figure 24). Type 5 dimensions were used for PETG, PLA, CuPLA and the z-orientation samples of EEL. Type 4 dimensions were used for the z-orientation samples of EEL.

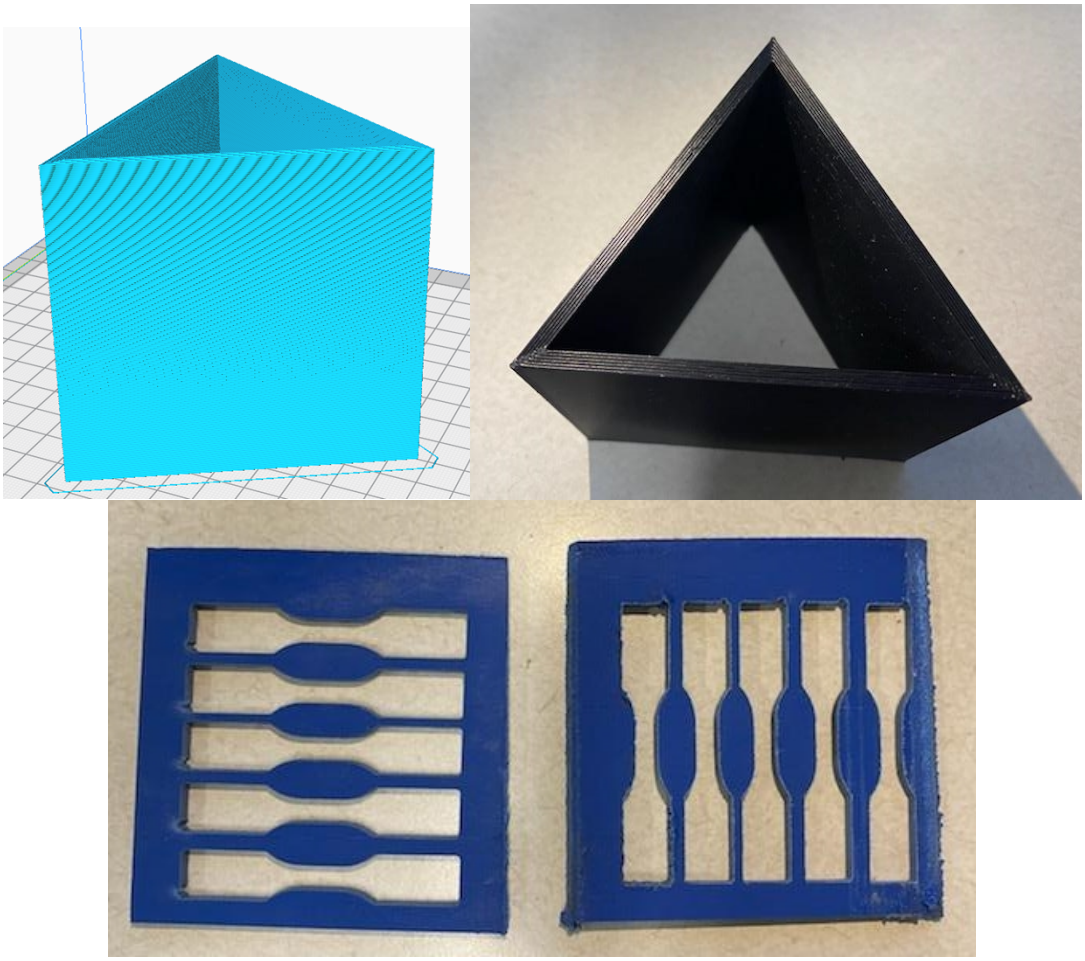

Figure 24: Examples of sliced geometry to print (top left), printed geometry (top right), and cut panels with samples waterjet out: x-orientation (bottom left) and z-orientation (bottom right).

For the samples of conductive materials (CuPLA and EEL), conductive leads of copper tape were epoxied to each end of the sample, outside of both the grip area and the area expected to fail. The epoxy used was CW2400. For all samples, reflective tape was attached to each sample at the extents of the area expected to fail. See example in Figure 25 below.

Figure 25: Example of a prepared conductive sample with leads and reflective tape attached.

Testing and Data Collection: The machine used to test these samples was an MTS Criterion Model 45. Each sample was tested to failure at 1mm/min, except for the EEL x-orientation samples which were tested at 2mm/min until the extensometer could no longer measure the extension. The extensometer used was a LX500 by MTS. Data from the testing machine was logged at 10Hz using the designated software for the machine. In each test, the sample was loaded into the grips and a light preload was exerted on the sample between 30 and 100N.

Results and Trends: The tests can be clustered into eight groups based on material and orientation: (1) PLA x-orientation, (2) PLA z-orientation, (3) CuPLA x-orientation, (4) CuPLA z-orientation, (5) PETG x-orientation, (6) PETG z-orientation, (7) EEL z-orientation, and (8) EEL x-orientation. Observations, trends, and results for each group are detailed below:

(1) *PLA x-orientation:* One sample broke outside the tape, and another slipped out of the grips and therefore didn't fail. The other three exhibited an average elastic modulus of 2.81GPa with a standard deviation of 0.54GPa, and an average ultimate tensile strength of 51.11MPa with a standard deviation of 0.20MPa. Although our testing cannot be considered statistically significant, these x-orientation tensile measurements seem to align with published figures for printed PLA specimens [1].

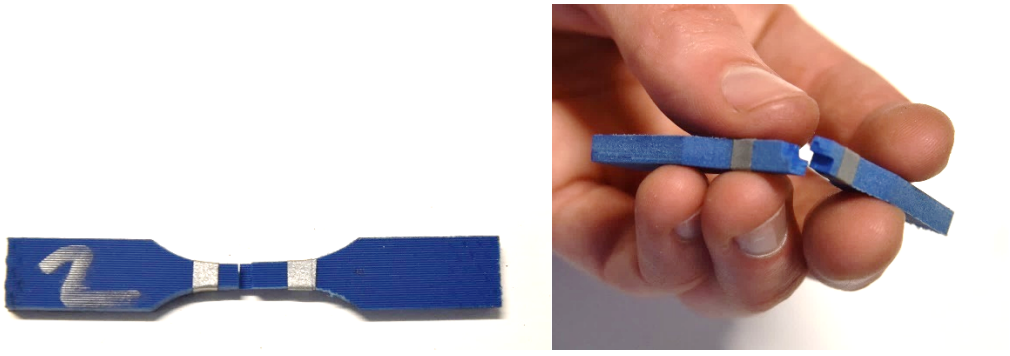

Figure 26: Example of tested PLA x-orientation sample.

(2) *PLA z-orientation:* One sample broke outside the tape, while two others broke on the tape. For the four that broke on or within the tape, the average elastic modulus exhibited was

2.05GPa with a standard deviation of 0.32GPa, and an average ultimate tensile strength of 26.97MPa with a standard deviation of 2.16MPa.

Figure 27: Example of tested PLA z-orientation sample.

(3) *CuPLA x-orientation:* Only one sample broke inside the gauge. Ten samples were tested, with six failing in nearly identical locations just above the tape and toward the bottom clamp. One sample had significant interlaminar blow-out from the water jet. Only one sample was successfully tested, showing an elastic modulus of 1.21GPa and an ultimate tensile strength of 12.96MPa.

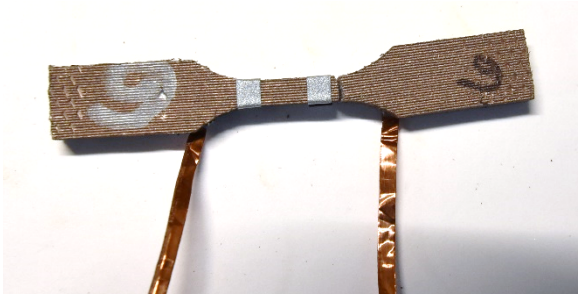

Figure 28: Example of tested CuPLA x-orientation sample.

(4) *CuPLA z-orientation:* Three samples broke prior to loading or during preloading, thus yielding no useful data. Only one sample was successfully tested, showing an elastic modulus of 0.65GPa and an ultimate tensile strength of 1.57MPa.

Figure 29: Example of tested CuPLA z-orientation sample.

(5) *PETG x-orientation:* No anomalies were observed during testing. A markedly ductile failure surface was observed for all samples. The average elastic modulus across all five samples was 1.95GPa with a standard deviation of 0.40GPa, while the average ultimate tensile strength was 42.73MPa with a standard deviation of 0.81MPa.

Figure 30: Example of tested PETG x-orientation sample.

(6) *PETG z-orientation:* All samples broke at an interlaminar boundary on what appears to be the same layer. This failure happened approximately on the tape. The average elastic modulus across all five samples was 1.39GPa with a standard deviation of 0.17GPa, while the average ultimate tensile strength was 20.47MPa with a standard deviation of 1.49MPa.

Figure 31: Example of tested PETG z-orientation sample.

(7) *EEL z-orientation:* All samples broke prior to or during loading, thus yielding no useful data.

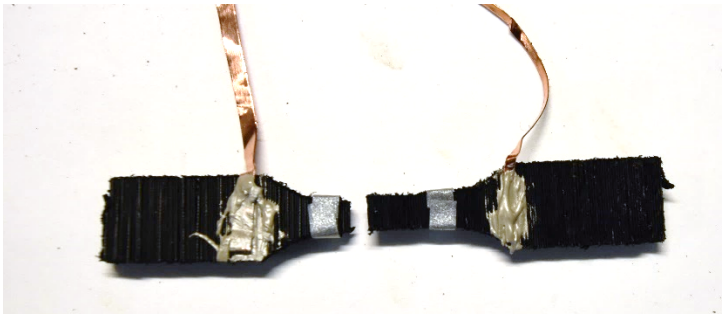

Figure 32: Example of broken EEL z-orientation sample.

(8) *EEL x-orientation:* Only two samples were tested as these samples stretched further than the extensometer could measure without failing. Interlaminar delamination was observed at the extents of the sample's deformation, as shown in Figure 33 below near the top grip. Each sample was stretched more than 30mm without failing.

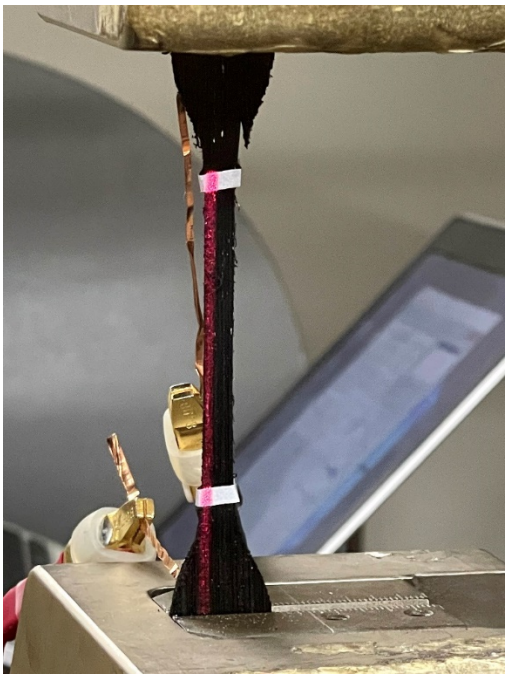

Figure 33: Example of EEL x-orientation sample during testing. Note extensometer laser is nearing the top of the top reflective tape and shortly afterward could not measure extension anymore.

Conclusions: The properties measured for neat PLA and PETG are aligned with values found in literature. During printing, water and humidity absorption played a particularly significant role in the printability of the CuPLA and EEL materials. We surmise that the sample preparation methods used may have impacted the performance of these samples, especially for EEL z-orientation variants. Development around the sample preparation methods to reduce interaction with water or excess humidity may lead to better outcomes. Further testing is required to confirm and quantify statistically significant results. Differences in elastic modulus, yield strength, and ultimate tensile strength between dielectric and conductive materials may have contributed to anomalous strain gauge behavior seen in prior experiments. Delamination or lack of adhesion between the dielectric and conductive materials may also be a contributing factor to this behavior.

Design of test article:

The design for a printed rib with embedded printed strain sensors was created in anticipation of printed gauge performance characterization. Eight gauges were embedded in each of the two shells of the rib conformal to the rib curvature, as seen in Figure 34.

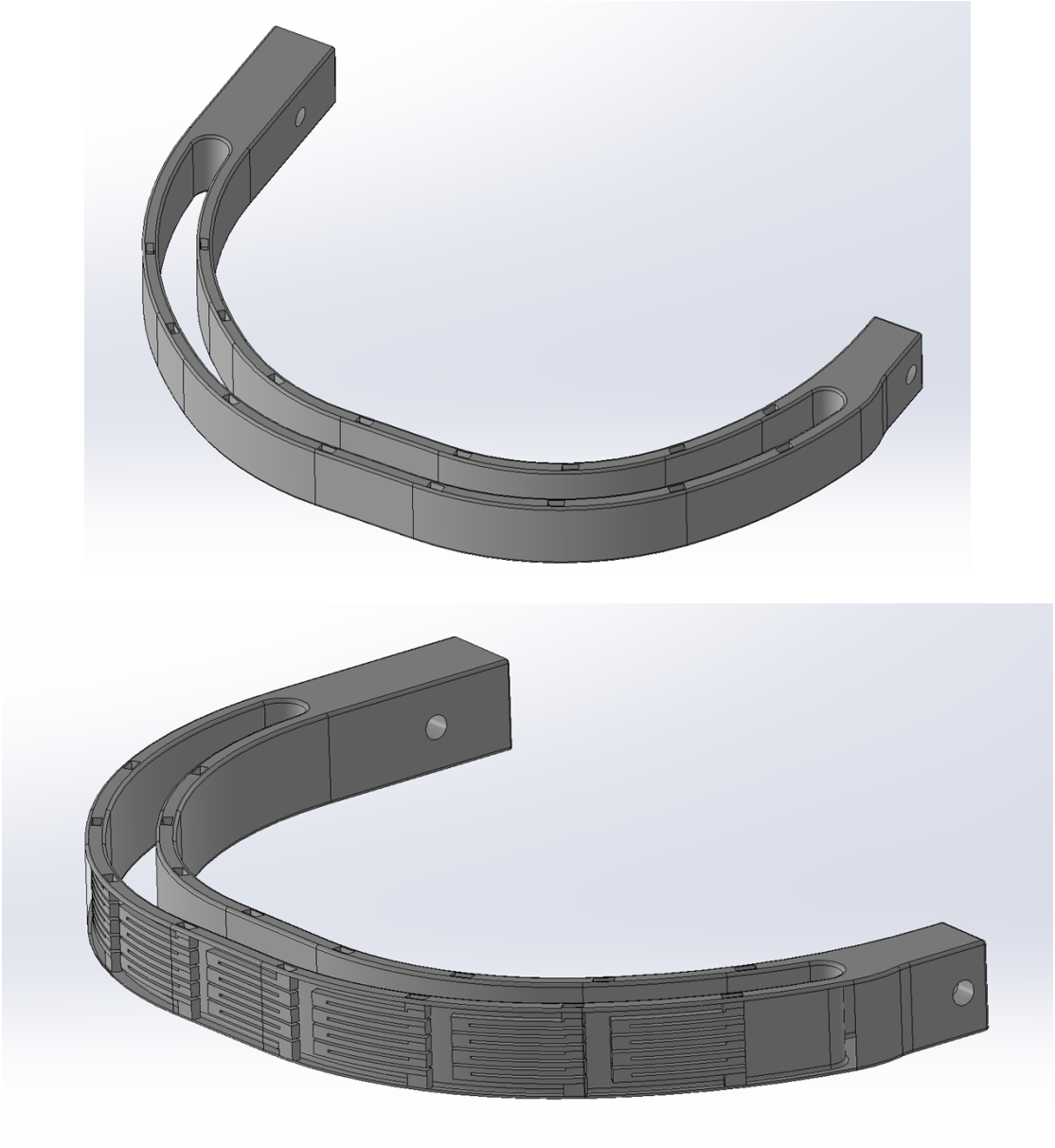

Figure 34: Test article designed, shown solid (above) and with transparent faces to show internal embedded gauges (below).

Literature Search:

A literature search was conducted to investigate prior work which might explain the nonlinear resistive response to tensile strain and the unexpected resistive response to compressive loads. Central questions asked throughout this literature survey were: how does electrical conduction happen in polymeric materials—particularly those similar to what we used in our study? What prior work has successfully demonstrated flexible or stretchable strain gauges with polymer-based materials? What manufacturing methods and sensing mechanisms have been employed for sensing strain or deformation in non-rigid applications? Our search surfaced: a taxonomy of different electrically conductive polymers, the concepts of percolation theory governing electrical conduction in conductive polymer composites such as the CuPLA and EEL materials used in this work, and many examples of flexible and stretchable sensors based on polymeric materials. The complete findings of this literature survey are planned to be published in a journal review article

Additional work with Humanetics

Printing Bumper for Testing

A bumper was printed using a TPU on the BAAM system. The bumper is to be used for testing the impact of vehicles on low objects. The bumper was sent to Humanetics where it was mounted to a test frame and tested in a crash test. The tests successfully demonstrated the functionality of the bumper. The bumper will be used in future vehicle testing.

Figure 35 Bumper testing is shown, before impact (left) and during impact (right)

Hand Mold Print Attempts

Humanetics required high temperature molds for molding the hands of the ATDs. They wished to explore the possibility of printing high temperature materials with a very fine layer resolution that would enable them to forego the machining phase of the manufacturing process. We tried printing with the high temperature polymer, PEKK, which we have at the MDF, but were unable to obtain satisfactory results at the desired layer thickness. We encountered problems with delamination at the very thin layer thicknesses and were unable to successfully print the mold.

4. SUBJECT INVENTIONS

Journal Review article is currently being written that discusses the findings of the literature survey performed on the manufacturing of strain gauges with every high strain and the materials and techniques that could be used to additively manufacture them.

5. COMMERCIALIZATION POSSIBILITIES

Humanetics has interest in using this technology to embed strain gauges into their additively manufactured anthropomorphic test dummies. They are actively pursing partners to synthesize materials for testing. Once materials are found they will integrate this into their AM ATDs. The increased fidelity of data that can be collected from these dummies will have significant impacts on the crash test industry and vehicle safety and design. Humanetics has significant interest in the successful development of this technology.

6. PLANS FOR FUTURE COLLABORATION

Humanetics has expressed interested in continuing to collaborate after they do testing and analysis of some of the materials and manufacturing techniques highlighted in our literature survey. Once suitable material has been determined, we may work with them on the design, printing and integration of the sensors into the AM ATDs.

7. CONCLUSIONS

The results of the project showed that several commercially available off the shelf conductive polymers are not able to meet the minimum specifications for strain in ATDs. The materials tested exhibited anomalous behavior that was likely attributed to plastic deformation during displacement. Designs of printable strain gauges both embedded and surface mounted exhibited this behavior, suggesting that new materials must be developed for the strain gauge to work in the desired strain range. A detailed literature survey was performed exploring material types and manufacturing methods for high strain flexible strain gauges. This literature survey will inform the next phase of development including the development of novel printable conductive materials and applications of new deposition methods. The development of these new materials and methods will enable the manufacturing of ATDs with significantly higher fidelity data output. This will have significant impact on crash testing and vehicle design, improving the safety of vehicles.

8. REFERENCES

[1] S. Brischetto and R. Torre, "Tensile and Compressive Behavior in the Experimental Tests for PLA Specimens Produced via Fused Deposition Modelling Technique," *Journal of Composites Science,* vol. 4, no. 3, 2020, doi: 10.3390/jcs4030140.